RSC Advances

PAPER

View Article Online
View Journal | View Issue

Cite this: *RSC Adv.*, 2025, **15**, 15801

Hybrid dansyl-triazine based mono and bidentate ligands for the selective sensing of fluoride anion through fluorescence enhancement†

Ajay Jayaprakash, ‡[a] Rakhi Mol K. M. ‡[a] and Mintu Porel *[ab]

Received 14th February 2025
Accepted 5th May 2025

DOI: 10.1039/d5ra01092f

rsc.li/rsc-advances

The design and synthetic strategy of hybrid mono and bidentate dansyl-triazine ligands (**DTM** and **DTD**) for selective sensing of fluoride anion are reported. The synthesised compounds were characterised using spectroscopic techniques such as ^{1}H NMR, LC-MS, IR, UV-vis absorption and emission and corroborated with theoretical methods. Studies showed that the bidendate ligand (**DTD**) exhibits intra-molecular charge transfer (ICT) from the donor dansyl fluorophore (HOMO) to the triazine acceptor (LUMO). On the other hand, electron density of the HOMO and LUMO of the mono ligand is localised on the dansyl group. Interestingly, these ligands showed selective detection of fluoride anions with a limit of detection (LOD) of 1.31 μM and 294 nM for the **DTM** and **DTD** ligands respectively. The electrostatic potential surface mapping suggests that the hydrogen bonding between NH of the ligand and fluoride ion as the underlying mechanism for sensing. Time-correlated single photon counting (TCSPC) analyses further validate this rationale, where **DTM** showed a lifetime of 3.56 ns and **DTD** 1.65 ns. Upon binding, the lifetime increases, this may be attributed to the restricted molecular rotation upon hydrogen bonding.

1. Introduction

Fluoride plays a vital role in human health and environmental systems, making its detection a blooming area of research.[1,2] It is widely known for its advantageous properties such as preventing tooth decay[3] and strengthening enamel.[4] However, excessive exposure of fluoride ions can lead to major health issues such as dental and skeletal fluorosis. Apart from the health effects, fluoride contamination in water bodies[5,6] poses detrimental environmental issues, as it enters the food chain and creates hazards that require timely attention.[7] The World Health Organization (WHO) has established a permissible limit of 1.5 mg L^{-1} fluoride in drinking water to prevent adverse effects. So, monitoring fluoride concentrations with precision is essential to ensure its benefits and to mitigate its risk factors.

Traditional methods used for fluoride detection are chromatographic techniques,[8] spectral titrations,[9–11] and electrochemical methods.[12–14] These procedures often require specialized equipment and are time consuming. Those limitations have motivated researchers for the development of advanced sensing technologies, especially chemosensors and fluorosensors, for rapid and cost-effective fluoride detection both quantitatively and qualitatively.[15] The sensing approaches involves different mechanisms such as photoinduced electron transfer (PET),[16] intramolecular charge transfer (ICT),[17,18] and hydrogen bonding[19,20] to achieve high selectivity and sensitivity for fluoride anions.

Recent research has focused on designing fluoride-specific probes with diverse chemical and structural probes such as azo compounds,[21] rhodamine derivatives,[22] Schiff bases,[23,24] and coumarin-based[25,26] fluorophores. These sensors exploits interactions distinctive to fluoride ions, such as strong hydrogen bonding and deprotonation, which in turn can induce measurable optical or fluorescence changes. For instance, coumarin **A** (Fig. 1) and polymer-based probes are being used for detecting fluorides.[25,27,28] This was found to offer rapid

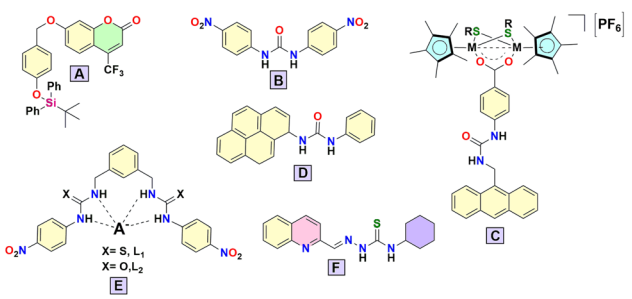

Fig. 1 Representative examples of previously reported NH based fluoride anion sensors.

[a]*Department of Chemistry, Indian Institute of Technology Palakkad, Kerala 678557, India. E-mail: mintu@iitpkd.ac.in*

[b]*Environmental Sciences and Sustainable Engineering Centre, Indian Institute of Technology Palakkad, Kerala 678557, India*

† Electronic supplementary information (ESI) available. See DOI: https://doi.org/10.1039/d5ra01092f

‡ Authors contributed equally.

colorimetric and fluorometric responses. In the biomedical field, these sensors have shown potential for fluoride bioimaging, revealing intracellular dynamics with high precision.[29] Apart from the above molecular motifs urea and thiourea based sensors with NH units capable of acting as strong directional hydrogen bond donors can effectively bind with small, hard and highly basic fluoride anion. Boiocchi *et al.* showed that a 1,3-bis(4-nitrophenyl)urea molecule **B** (Fig. 1) forms highly stable hydrogen-bonded complexes with fluoride anion. Upon adding excess of fluoride, NH gets deprotonated generating HF_2^- and leading to significant colorimetric changes.[30] Similarly, Zhou *et al.* reported carboxylate-bridged diiron complexes bearing urea and anthracene units **C** (Fig. 1), which showed selective fluorescence enhancement upon F^- binding *via* N–H···F^- interactions.[31] Later Xia *et al.* provided mechanistic insight through TDDFT calculations, revealing that the interaction of 1-phenyl-3-(pyren-1-yl)urea **D** (Fig. 1) with fluoride results in excited-state hydrogen bond strengthening, leading to non-radiative deactivation and a characteristic fluorescence response.[32] A urea and thiourea-functionalized *meta*-xylylene clefts **E** (Fig. 1), both exhibiting strong selectivity toward fluoride with clear colorimetric responses, attributed to directional hydrogen bonding and enhanced anion affinity due to increased acidity.[33] Quite recently, a quinoline-based fluorescent sensor **F** was found to selectively bind fluoride through N–H···F^- interaction and undergoes deprotonation, as confirmed by NMR and TD-DFT calculations (Fig. 1).[34] Also there are fluoride sensors, which are based on transition metals, silicon, imidazole and OH sensing units (Table S1†).

Though there is a remarkable progress in the field, challenges still remain in enhancing sensor stability, sensitivity, minimizing interference from other structurally similar ions, and improving scalability for large scale industrial applications. The synthesis of molecular probes can also be hindered by the poor yields of the reactions or tedious purification procedures. So, addressing these challenges will require novel materials and modern or sustainable methodologies, enabling the development of next-generation fluoride sensors with higher efficiency and versatility. Taking into consideration the stability, synthesis and detection difficulty without metal ions, we used well known precursors dansyl chloride and a triazine derivative to form a hybrid mono (**DTM**) and bidentate (**DTD**) ligands to achieve selective fluoride sensing. The extent of sensing depends on the number of NH units present in the molecule as well as the intramolecular charge transfer.

2. Experimental section

2.1 Synthesis of compounds DTM and DTD

To the 2,4-diamino-6-phenyl-1,3,5-triazine (1) (100 mg, 0.534 mmol, 1.0 equiv.) and sodium hydride (51.28 mg, 2.14 mmol, 4.0 equiv.), 2 mL of dimethyl formamide (DMF) was added and kept in an ice bath for 10 minutes. DMF solution of dansyl chloride (2) (360.24 mg, 1.34 mmol, 2.5 equiv.) was then added and stirred for 30 minutes. Progress of the reaction was monitored by TLC. The mixture was quenched with water and extracted with ethylacetate. Products **DTM** and **DTD** was isolated as white and yellow solid after silica gel column chromatography. The reaction yields for **DTM** and **DTD** were 24% (54 mg) and 59% (206 mg) respectively. MS (ESI) m/z: $[M + H]^+$ calcd for **DTM** ($C_{21}H_{20}N_6O_2S$) 421.14; found 421.35. MS (ESI) m/z: $[M + H]^+$ calcd for **DTD** ($C_{33}H_{31}N_7O_4S_2$) 654.19; found 654.50 **DTM**: ^{1}H NMR (500 MHz, DMSO) δ 12.19 (broad singlet, NH), 8.51 (d, J = 7.2 Hz, 1H), 8.44 (t, J = 9.2 Hz, 1H), 8.37 (t, J = 10.7 Hz, 1H), 8.01 (d, J = 7.5 Hz, 2H), 7.73 (t, J = 7.9 Hz, 1H), 7.63–7.52 (m, 3H), 7.51–7.29 (m, 3H), 7.20 (t, J = 11.4 Hz, 1H), 2.78 (s, 6H). ^{13}C NMR (101 MHz, DMSO) δ 172.5, 153.3, 134.3, 131.0, 130.7, 130.3, 130.1, 129.8, 125.4, 120.9, 116.9, 47.0, 22.7. **DTD**: ^{1}H NMR (400 MHz, DMSO) δ 12.13 (broad singlet, NH), 8.50 (d, J = 7.2 Hz, 2H), 8.39 (d, J = 8.5 Hz, 2H), 8.31 (d, J = 8.7 Hz, 2H), 7.72 (t, J = 8.0 Hz, 4H), 7.54 (dt, J = 14.6, 7.6 Hz, 3H), 7.40 (t, J = 7.6 Hz, 2H), 7.20 (d, J = 7.6 Hz, 2H), 2.76 (s, 12H). ^{13}C NMR (101 MHz, DMSO) δ 172.4, 163.8, 152.4, 132.9, 131.5, 130.7, 130.6–130.2, 129.9, 125.6, 121.1, 117.2, 46.9, 32.8, 23.9, 15.9.

2.2 Photophysical and sensing study

For UV-vis absorption and emission studies, 2 mM stock solutions of the compounds (**DTM** and **DTD**) were prepared in DMSO, and 20 μM solutions were used for spectral measurements. For selectivity studies, 10 μM sensor solutions were prepared, and fluorescence spectra were recorded after adding 100 μM of various anions (all the anion have same counter cations; the tetrabutyl ammonium). The limit of detection was determined using the $3\sigma/K$ method, where σ represents the standard deviation and K denotes the slope of fluorescence intensity *versus* fluoride anion (F^-) concentration. For competition studies, fluorescence spectra were recorded before and after sequentially adding different anions, followed by fluoride.

2.3 Computational study

All calculations were carried out using the Gaussian 16 program package. Calculations were performed by the density functional theory (DFT) method with restricted B3LYP (Becke's three-parameter hybrid exchange functional and the Lee–Yang–Parr correlation functional) level, employing a basis set 6-31G (d). Firstly the geometries of the free ligands were optimised and the energies are calculated with imaginary frequency as zero. Then the fluoride binding studies were computed and the electrostatic potentials are generated using Gauss-View.

3. Results and discussion

The synthetic strategy involves nucleophilic substitution reaction between the key building blocks 2,4-diamino-6-phenyl-1,3,5-triazine **1** and dansyl chloride **2**. Molecules **1** and **2** in the presence of sodium hydride (NaH) as the base in dimethylformamide (DMF) at 0 °C affords mono substituted **DTM** and disubstituted **DTD** product in 24% and 59% yields respectively (Scheme 1). Initial confirmation of the synthesised molecules were performed using the LC-Mass analyses. For compound **DTM**, it showed a molecular ion peak at 421.35 Da (calculated for $C_{21}H_{20}N_6O_2S$ $[M + H]^+$, m/z = 421.14) and

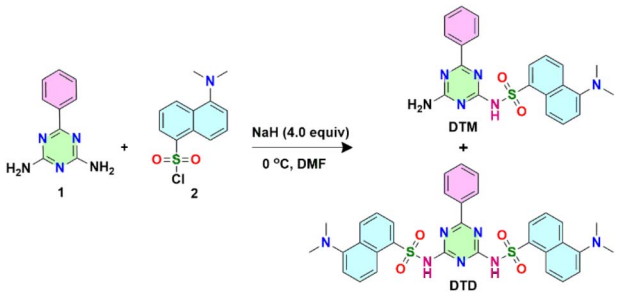

Scheme 1 Synthesis of DTM and DTD.

compound **DTD** at 654.50 Da (calculated for $C_{33}H_{31}N_7O_4S_2$ $[M + H]^+$, $m/z = 654.19$) (Fig. 2a, S1 and S2†). The Fourier Transform Infrared spectra showed a characteristic NH of the sulphonamide group and a NH_2 peak for compound **DTM**, on the other hand a broad peak corresponding to two NH of the sulphonamide moiety were obtained for **DTD** (Fig. 2c).

The ^{1}H-NMR spectra for the molecules were recorded in DMSO-d_6 at 298 K (Fig. S3–S10†). For **DTM**, the protons corresponding to the phenyl ring of the triazine moiety exhibited a doublet at 8.02 ppm (type i) showed correlations with two multiplets centered at 7.46 and 7.55 ppm (type e, d). The aromatic protons correlating with each other from 7.21 ppm to 8.52 ppm (type a, c, h, f, g, j) is attributed to the dansyl ring and the six protons of the *N*,*N*-dimethyl unit without any correlations showed a singlet at 2.78 ppm (type k). The NH_2 unit resonated at 7.46 ppm and the NH appeared as a broad singlet at 12.19 ppm (Fig. 2b and S3–S5†). On the other hand, as expected **DTD** showed a relatively simple spectrum when compared to **DTM** due to its highly symmetric nature. The twelve protons corresponding to the two *N*,*N*-dimethyl substituent exhibited a sharp singlet at 2.76 ppm (type j) and the other aromatic dansyl protons showing multiple correlations in the ^{1}H–^{1}H COSY resonated in the range from 7.19 ppm to 8.51 ppm (type a–f) respectively. The phenyl protons of the triazine ring exhibiting two correlations appeared in the range from 7.42 ppm to 7.69 ppm (type g, h, i). There is no NH_2 signal present in the **DTD** and the two NH's appeared as a singlet at 12.13 ppm. A slight deshielding of the dansyl protons and a shielding of the phenylene proton of the triazine ring in **DTD** when compared to **DTM**, indicates the presence of charge transfer from the donor dansyl fluorophore to the acceptor triazine moiety (Fig. S7–S9†).

The electronic absorption and emission spectra of the synthesized molecules were recorded in DMSO at 25 °C. The UV-vis absorption spectra of **DTM** showed maxima peaks at 286 and 326 nm and **DTD** at 288 and 327 nm (Fig. 2d, S11 and S12†). Molecules when excited at 326 nm exhibited an emission maxima of 481 nm and 462 nm for **DTM** and **DTD** respectively (Fig. 2d, S11 and S12†). Quantum yield for the ligands with respect to quinine sulphate in DMSO is 0.40 for **DTM** and 0.22 for **DTD**. The reduction in quantum yield for **DTD** when compared to **DTM** may be attributed to the intramolecular charge transfer.

The presence of NH in the sulfonamide moiety of the molecules were further exploited for anion sensing applications in DMSO solution. We have screened various anions like F^-, Cl^-, Br^-, I^-, BF_4^-, PF_6^-, SCN^-, HSO_4^- and $H_2PO_4^-$, where its counter cation is tetrabutyl ammonium. Interestingly, both **DTM** and **DTD** showed fluorescence enhancement when tetrabutyl ammonium fluoride was added to the solution. On the other hand, remaining analytes did not show any enhancement in the emission intensity illustrating the selectivity of the molecules towards fluoride ion (Fig. 3c, S13 and S14†). To further investigate the extent of interaction of fluoride with these sensors, fluorescence titration experiments were carried out. Upon adding 0–100 μM solution of fluoride ion to **DTM** and **DTD**, a minimal fluorescence enhancement was observed for **DTM** whereas a 2.5-fold enhancement for **DTD** (Fig. 3a and

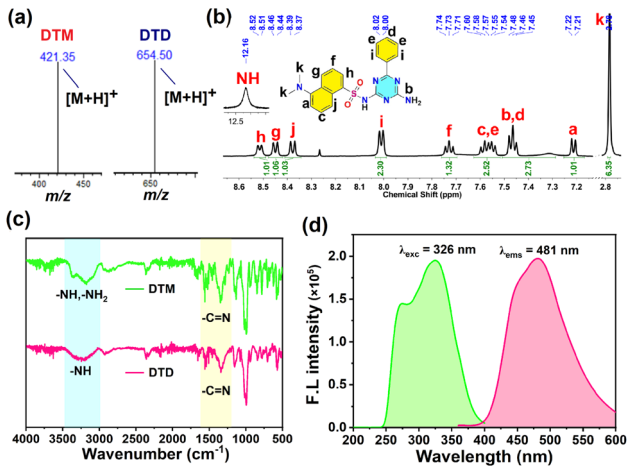

Fig. 2 (a) Mass spectra of **DTM** and **DTD** (b) ^{1}H-NMR spectra of **DTM** (400 MHz, DMSO-d_6) (c) FT-IR spectra of **DTM** (top) and **DTD** (bottom) (d) normalised excitation and emission spectrum of **DTM**.

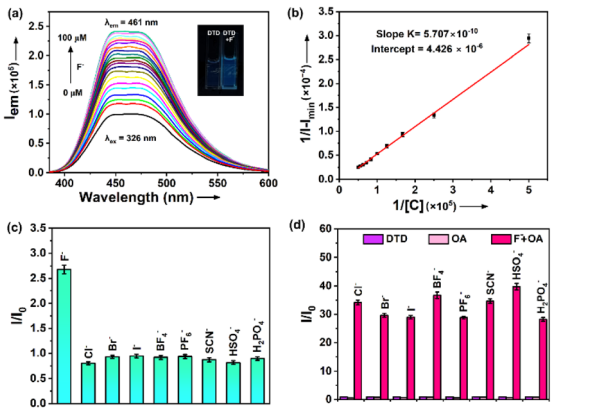

Fig. 3 Studies for the detection of fluoride ion using **DTD**: (a) changes in the fluorescence profile upon titration with various concentration of fluoride ion (0 μM to 100 μM) when excited at 326 nm in DMSO; inset shows the cuvette images of the probe **DTD** with and without fluoride ions (b) Benesi–Hildebrand plot obtained from the titration of **DTD** with fluoride ion (c) bar diagram showing the selectivity for picric acid in the presence of other anions, (d) bar diagram representing competition in the presence of various anions (OA = other analytes).

S15†). To obtain the binding constant and to substantiate the fluoride interaction Benesi–Hildebrand method was employed (Fig. 3b, S20 and S21†). The binding constant (K_a) value calculated for **DTM** and **DTD** was $(3.68 \pm 0.14) \times 10^2\ M^{-1}$ and $(7.75 \pm 0.71) \times 10^3\ M^{-1}$ respectively. The limit of detection (LOD) values obtained using the $3\sigma/K$ method were 1.31 μM (±0.77 μM) for **DTM** and 293.6 nM (±0.28 nM) for **DTD** (Fig. S16–S19†). Binding constant along with the LOD values suggest that **DTD** binds fluoride more strongly when compared to **DTM**. This may be due to the presence of two NH-sulfonamide groups in **DTD** when compared to one NH-sulfonamide in **DTM**. We have carried out the competivity studies for the molecular probes in the presence of other analytes (Fig. 3d and S22†). It is evident that the sensor binds fluoride ions selectively with fluorescence enhancement in presence of other analytes. The cuvette images showed that under the UV lamp, the bare **DTD** showed minimum fluorescence and adding fluoride solution increases the emission intensity. ^{1}H NMR spectral titrations of **DTM** and **DTD** with one equivalent of tetrabutylammonium fluoride revealed the disappearance of broad NH singlets, indicative of hydrogen bonding interactions between the fluoride anion and the NH groups of the sensor molecules in a 1 : 1 binding mode. This observation was corroborated by the upfield shift of the aromatic dansyl proton signals. Notably, the magnitude of the shift was more pronounced in **DTD** than in **DTM**, suggesting a stronger binding affinity of **DTD** towards fluoride (Fig. S6 and S10†). Further, time-correlated single photon counting analyses were carried out for the free ligands as well as after adding 50 μM fluoride solution. For **DTM** the life time was found to be 3.56 ns (±0.01 ns) and **DTD** the life time was 1.65 ns (±0.04 ns). On adding fluoride ion the life time increases to 6.23 ns (±0.03 ns) for **DTD**, whereas no considerable change was observed for **DTM** (Fig. S23 and S24†). This may be attributed to the strong hydrogen bonding interaction, leading to restricted molecular rotation.

To demonstrate the applicability of this sensor in real-time analysis, we have carried out the sensing studies in deionised water (Fig. S25†). Upon adding tetrabutyl ammonium fluoride to **DTD**, as expected there is an enhancement in the fluorescence intensity, on contrary other anions did not showed any change in the emission spectra. Similarly in the case of **DTM**, there was only a minimal fluorescence enhancement upon adding fluoride source, and no changes were observed with other anions. Further, instead of deionised water we have taken lake, pond and tap water and spiked known concentration of fluoride source (50 μM) to it. Then we monitored the sensing of fluoride ion using **DTD**. It was observed that in all the cases the emission intensity increases showing its applicability in real-life scenarios (Fig. S26†). In addition to that we have also developed a paper strip sensor using the **DTD** sensor. When ligand **DTD** was drop-casted onto Whatman filter paper and observed under a UV lamp, no fluorescence was initially detected. However, upon the addition of a fluoride ion source, the fluorescence intensity increased significantly showing simple optical detection (Fig. S27†). The increase in emission intensity of **DTD** (**DTM**) upon fluoride binding is attributed to hindrance of intramolecular charge transfer (ICT) in the dansyl fluorophore. The fluoride ion after binding to NH can impart a partial negative charge to the nitrogen atom. This can effectively participate in conjugation with the sulphonyl group and disrupts the conjugation from *N*,*N*-dimethyl unit in the dansyl fluorophore leading to enhanced fluorescence (Fig. S28†).

To gain deeper insights into the structure and electronic properties of the synthesised compounds, density functional theory calculations were employed at the B3LYP-6-31G(d) level of theory. The optimised structure of the molecules showed non-planar structures. The theoretical HOMO–LUMO gaps were found to be 4.05 eV and 3.93 eV for compound **DTM** and **DTD** respectively (Fig. 4a and b). Curiously, the mono-dentate ligand **DTM** showed localisation of charge densities on the dansyl fluorophores in the HOMO and LUMO level. On the other hand, the HOMO of the bidentate ligand **DTD** is on the donor dansyl group and the LUMO is on the acceptor triazine moiety indicating an intra-molecular charge transfer, reduced quantum yield as well as validating the reduced energy gaps. Upon fluoride binding, the energy gap of the compound **DTM** decreases to 4.02 eV, and intriguingly showed an intramolecular charge transfer from dansyl to the triazine core. Similarly the bidentate ligand also displayed a reduced energy gap of 3.67 eV after binding with fluoride anion (Fig. 4a and b). To further probe the mechanism of binding, we have mapped the electrostatic potential surfaces for both the ligands. The surfaces suggests that the blue regions are on the NH_2 and NH groups. Compound **DTM** have both NH_2 and sulphonamide NH groups, whereas **DTD** have two sulphonamide NH groups. Due to the acidity of NH group, the fluoride anion can have strong hydrogen bonding interactions with bidentate ligand when compared to mono substituted product. The H–F hydrogen bond distance calculated is found to be 2.02 Å is in agreement with the strong interactive nature (Fig. 4c and d).[35]

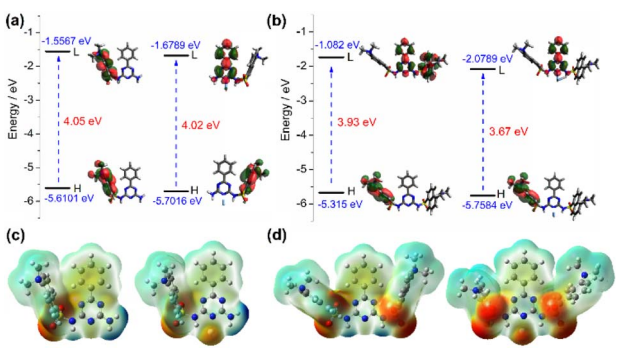

Fig. 4 Energy level diagram and Electrostatic Potential Surface (ESP) of – (a) DTM, (b) DTD (c) DTM + F^-, (d) DTD + F^-.

4. Conclusions

In conclusion we have strategically designed and synthesised two molecular probes **DTM** and **DTD** using simple nucleophilic substitution reaction of dansyl chloride with a 2,4-diamino-6-phenyl-1,3,5-triazine in good yields. The molecules showed high quantum yield, 0.40 for **DTM** and 0.22 **DTD**. The reduction

in quantum yield for **DTD** when compared to **DTM** is due to the intramolecular charge transfer from the dansyl donor to the triazine acceptor. The presence of sulphonamide NH moiety in the **DTM** and **DTD** ligands were explored for the sensing of various anions. Sensing studies revealed that the molecules binds fluoride anion selectively as evident from the titration experiments, binding constant (K_a), LOD and competivity analyses. Notably there is a 4 fold enhancement in LOD for the **DTD** when compared to **DTM**. Density Functional Theory calculations corroborated well with the experimental results. Electrostatic potential surfaces for the **DTM** and **DTD** showed strong hydrogen bonding interactions with the fluoride ion, underlying the sensing mechanism. This is also evident from the increased lifetime of the ligands after adding fluoride ions. The applicability of **DTM** and **DTD** for real sample analysis was evaluated using lake, pond, and tap water samples, and a paper strip-based sensor was subsequently developed. However the limited solubility of **DTM** and **DTD** in few solvents presents ongoing challenges for their deployment in practical applications. To mitigate these limitations, structural modifications focusing on the triazine core are being systematically explored in our laboratory and their potential applications will be explored further.

Data availability

The authors confirm that the data supporting the findings of this study are available within the article and/or it's ESI.†

Conflicts of interest

There are no conflicts to declare.

Acknowledgements

M. P. thanks Exploratory Research Grant, Indian Institute of Technology Palakkad, India (2024-230-CHY-MIP-ERG-SP) for funding. A. J. thanks Indian Institute of Technology Palakkad, India for the Post-Doctoral Research Fellowship. R. K. M. thanks UGC-JRF India for fellowship.

Notes and references

1 Y. Zhou, J. F. Zhang and J. Yoon, *Chem. Rev.*, 2014, **114**, 5511.
2 A. Dhillon, M. Nair and D. Kumar, *Anal. Methods*, 2016, **8**, 5338.
3 C. M. Carey, *J. Evid. Base Dent. Pract.*, 2014, **14**, 95.
4 F. J. Aulestia, J. Groeling, G. H. S. Bomfim, V. Costiniti, V. Manikandan, A. Chaloemtoem, A. R. Concepcion, Y. Li, L. E. Wagner, Y. Idaghdour, D. I. Yule and R. S. Lacruz, *Sci. Signaling*, 2020, **13**, 1.
5 S. Ahmad, R. Singh, T. Arfin and K. Neeti, *Environ. Sci.:Adv.*, 2022, **1**, 620.
6 E. Shaji, K. V. Sarath, M. Santosh, P. K. Krishnaprasad, B. K. Arya and M. S. Babu, *Geosci. Front.*, 2024, **15**, 101734.
7 S. Wu, Y. Wang, M. Iqbal, K. Mehmood, Y. Li, Z. Tang and H. Zhang, *Environ. Pollut.*, 2022, **304**, 119241.
8 G. Yamamoto and K. Yoshitake, *Anal. Chim. Acta*, 1989, **222**, 121.
9 X. Wu, H. Wang, S. Yang, H. Tian, Y. Liu and B. Sun, *ACS Omega*, 2019, **4**, 4918.
10 M. Rizal B, N. Mudasir and F. I. Pambudi, *RSC Adv.*, 2024, **14**, 31143.
11 T. Feng, J. Yang, Y. Wang, T. Hu, L. Yan and Y. Le, *Anal. Methods*, 2025, **17**, 939–943.
12 R. Appiah-Ntiamoah, B. T. Gadisa and H. Kim, *New J. Chem.*, 2018, **42**, 11341.
13 L. M. Novak and E. M. Steyskal, *RSC Adv.*, 2023, **13**, 6947.
14 M. Thiruppathi, T. Natarajan and J. M. Zen, *J. Electroanal. Chem.*, 2023, **944**, 117685.
15 S. Chakraborty, *Results Chem.*, 2023, **6**, 100994.
16 S. K. Kim and J. Yoon, *Chem. Commun.*, 2002, **2**, 770.
17 T. Samanta, N. Das and R. Shunmugam, *ACS Sustain. Chem. Eng.*, 2021, **9**, 10176.
18 G. Sivakumar, A. Babu, A. Das, M. Anandhan, V. Nutalapati and S. Maji, *Mater. Adv.*, 2024, **5**, 8909.
19 R. Manivannan, A. Satheshkumar and K. P. Elango, *New J. Chem.*, 2013, **37**, 3152.
20 C. Mahapatra, S. Samanta, S. Diyali, B. Biswas, S. Paul, T. Majumder and A. Mallick, *J. Photochem. Photobiol., A*, 2024, **459**, 116024.
21 H. Khanmohammadi and K. Rezaeian, *RSC Adv.*, 2014, **4**, 1032.
22 G. Sivaraman and D. Chellappa, *J. Mater. Chem. B*, 2013, **1**, 5768.
23 A. A. Mahishi, S. M. Shet, P. V. Mane, J. Yu, A. V. Sowriraajan, M. Kigga, M. P. Bhat, K. H. Lee and M. D. Kurkuri, *Anal. Methods*, 2023, **15**, 3259.
24 B. R. Jali and J. B. Baruah, *Dyes Pigm.*, 2021, **194**, 109575.
25 B. R. Swain and R. Satapathy, *Tetrahedron*, 2023, **134**, 133310.
26 S. Amer, V. Joseph, B. El Oded, V. Marks, F. Grynszpan and M. Levine, *Org. Biomol. Chem.*, 2023, **21**, 9410.
27 Q. Zhao, C. Zhang, S. Liu, Y. Liu, K. Y. Zhang, X. Zhou, J. Jiang, W. Xu, T. Yang and W. Huang, *Sci. Rep.*, 2015, **5**, 1.
28 W. Zhang, G. Li, L. Xu, Y. Zhuo, W. Wan, N. Yan and G. He, *Chem. Sci.*, 2018, **9**, 4444.
29 R. Liu, Y. Gao, Q. Zhang, X. Yang, X. Lu, Z. Ke, W. Zhou and J. Qu, *New J. Chem.*, 2014, **38**, 2941.
30 M. Boiocchi, L. Del Boca, D. E. Gómez, L. Fabbrizzi, M. Licchelli and E. Monzani, *J. Am. Chem. Soc.*, 2004, **126**, 16507–16514.
31 Y. Zhou, X. Dong, Y. Zhang, P. Tong and J. Qu, *Dalton Trans.*, 2016, **45**, 6839–6846.
32 Y. Xia, M. Li, A. Xu, Z. Zhang, A. Sun, S. Ding an and Y. Liu, *Spectrochim. Acta, Part A*, 2021, **246**, 118992.
33 U. Manna, B. Portis, T. K. Egboluche, M. Nafis and M. A. Hossain, *Front. Chem.*, 2021, **8**, 1–7.
34 A. V. Ashwathi and S. M. Basheer, *Sci. Rep.*, 2025, **15**, 1859.
35 H. J. Schneider, *Chem. Sci.*, 2012, **3**, 1381.